Absolute Conductivity Reconstruction in Magnetic Induction Tomography Using a Nonlinear Method

Soleimani, Manuchehr and Lionheart, William

2006

MIMS EPrint: **2016.31**

Manchester Institute for Mathematical Sciences
School of Mathematics

The University of Manchester

Reports available from: http://eprints.maths.manchester.ac.uk/
And by contacting: The MIMS Secretary
School of Mathematics
The University of Manchester
Manchester, M13 9PL, UK

ISSN 1749-9097

Absolute Conductivity Reconstruction in Magnetic Induction Tomography Using a Nonlinear Method

Manuchehr Soleimani [*], William R.B Lionheart [†]

July 12, 2006

Abstract

Magnetic Induction Tomography attempts to image the electrical and magnetic characteristics of a target using impedance measurement data from pairs of excitation and detection coils. This inverse eddy current problem is nonlinear and also severely ill posed so regularization is required for a stable solution. A regularized Gauss-Newton algorithm has been implemented as a nonlinear, iterative inverse solver. In this algorithm one needs to solve the forward problem and recalculate the Jacobian matrix for each iteration. The forward problem has been solved using an edge based finite element method for magnetic vector potential **A** and electrical scalar potential V, a so called **A**, **A**-V formulation. A theoretical study of the general inverse eddy current problem and a derivation, paying special attention to the boundary conditions, of an adjoint field formula for the Jacobian is given. This efficient formula calculates the change in measured induced voltage due to a small perturbation of the conductivity in a region. This has the advantage that it involves only the inner product of the electric fields when two different coils are excited, and these are convenient computationally. This paper also shows that the sensitivity maps change significantly when the conductivity distribution changes, demonstrating the necessity for a nonlinear reconstruction algorithm. The performance of the inverse solver has been examined and results presented from simulated data with added noise.

Index term- Electromagnetic tomography, inverse problems, eddy currents, conductivity measurement.

1 Introduction

Magnetic induction tomography (MIT) is a potential modality for medical and industrial imaging (see for example [11], [15], [24], [29]). MIT attempts to infer interior conductivity distribution,

[*]William Lee Innovation Center, School of Materials and
[†]School of Mathematics, The University of Manchester, UK.

and possibly the distribution of other electromagnetic parameters, from mutual inductance measurements between coils exterior to the object. The technique operates as follows. Passing an alternating current through the excitation coil(s) produces an alternating magnetic field. The magnetic field induces a voltage in the sensing coils that is a nonlinear function of the electromagnetic properties. The reconstruction problem is to recover an approximation to the spatially varying electromagnetic properties from this data. The absence of direct electrical connections makes the technique of interest for non-invasive and non-intrusive applications. Potential applications of MIT for conductivity imaging in medical applications have been identified for example by [5] and [26]. In [5] and in [31] the possibility of using MIT for permeability imaging has also been investigated. In this paper we focus on electrical conductivity as the unknown. The formulation can be easily extended to complex conductivity reconstruction, but we will assume the permittivity and permeability distributions are given. Various image reconstruction techniques have been used for a similar inverse problem of medical electrical impedance tomography (EIT) [18, 25]. A mathematically similar problem (forward and inverse eddy current problem) has been studied extensively for Non-Destructive Testing (NDT) applications. Forward problem formulations, approaches to sensitivity analysis and inverse problem techniques have been developed for NDT by [8], [16], [22], [34]. Because of the differences in conductivity range and contrast in medical MIT, many of those techniques used in NDT may not be directly applicable here.

In medical MIT to date, a 'linear back projection' method [15] (similar to Kotre's method in EIT) and a single step regularized method [3] have been used. This paper further demonstrates the nonlinearity of MIT and show that the linear reconstruction methods are not generally adequate. It has been demonstrated earlier by [27] that the sensitivity map for a conductive background differs from the one for a free space background. The results of this paper demonstrate that the sensitivity map not only differs from that of free space but also changes significantly with the background conductivity distribution, so that it is essential to recalculate the Jacobian matrix at the iterative steps of the inverse solver.

Reconstruction of the conductivity requires a forward solver so that predicted data can be compared with measured data. We use an eddy current approximation to Maxwell's equations, which involves the computation of vector and scalar fields. The edge finite element method (edge FEM) has advantages over nodal elements for vector field computation in the eddy current problem [1]. Edge FEM has been employed for the medical and industrial MIT forward problem [20],[30]. Solving the forward problem of MIT using a scalar field has been reported by [9]. An eddy current formulation of $\mathbf{A}_r, \mathbf{A}_r - V$ presented by [20] models the electric field in the conducting region as sum of the scalar field V and primary magnetic vector potential, and a reduced magnetic vector potential $\mathbf{A}_r$.

We have implemented a flexible edge FEM eddy current program, specifically designed for MIT, for calculating the voltages induced in sensing coils when an excitation coil is driven, as well as the internal fields required for sensitivity computation. An efficient formulation for calculating the Jacobian matrix has been used. Sensitivity analysis of the system shows that even some large changes in the impedance of an object cause only small changes in the voltages induced in a coil.

Consequently the inverse problem is ill posed.

In common with many similar inverse boundary value problems for partial differential equations our problem is nonlinear, and beyond the small range of validity of a linear approximation it is necessary to use a reconstruction algorithm that reflects this. The regularized Gauss-Newton method uses repeated linearization to overcome the nonlinearity, and incorporates an *a priori* information about the unknown conductivity to obtain a stable solution of the inverse problem. The linearization, which is the Jacobian matrix or Fréchet derivative of the forward map, is an important part of such methods. A row of the Jacobian matrix can be interpreted as a map of the sensitivity of a given measurement to a small change in conductivity in each location. As we shall see in this paper these sensitivity maps depend strongly on the background conductivity about which the linearization is taken. This can be interpreted in several ways, one of which is that the second derivative is significant. In practice, while a linear reconstruction algorithm will often successfully locate an isolated inclusion in a homogeneous background, a nonlinear method is needed to reconstruct more complicated conductivity distributions, such as several nearby objects.

The forward problem is inherently three dimensional, and we show reconstructions of three dimensional objects. Simulated measurement data were generated using model phantoms, and Gaussian pseudorandom noise was added to the data. To further avoid 'inverse crimes' a different mesh was used in the inverse solution from the one used to create the simulated data. The software was designed to solve the forward problem and calculate the Jacobian for a general form of anisotropic material distribution, but the results presented in this paper are for isotropic materials. Our tetrahedral finite element meshes were made using a general purpose mesh generator provided by FEMLAB (Comsol AB, Stockholm). In any practical medical application one would need an accurate body-shaped mesh.

The paper is organized as follows. Section II studies the theoretical background of the inverse eddy current problem, and we derive the sensitivity formula in a general form. In section III a simple eight coil MIT system used for our simulation study is introduced. In section IV, the numerical implementation of the MIT forward problem is presented and in section V the numerical implementation of the sensitivity formula is described and a sensitivity analysis a presented. In section VI the formulation for the Gauss-Newton method will be reviewed and image reconstruction results for simulated data will be shown.

2 Theoretical study

2.1 Maxwell's Equations and MIT

Assuming time-harmonic fields with angular frequency ω Maxwell's equations are

$$\nabla \times \mathbf{E} = -\mathrm{i}\omega\mu\mathbf{H} \quad \nabla \cdot \mu\mathbf{H} = 0 \tag{1}$$

$$\nabla \times \mathbf{H} = (\sigma + \mathrm{i}\omega\varepsilon)\,\mathbf{E} + \mathbf{J}_s \quad \nabla \cdot \varepsilon\mathbf{E} = 0 \tag{2}$$

Here $\mathbf{E}$ and $\mathbf{H}$ are the magnetic and electric fields, σ is conductivity, μ magnetic permeability and ε permittivity. The current sources are represented by the current density $\mathbf{J}_s$. The inverse boundary value problem for Maxwell's equations is the recovery of the material parameters σ, ε and μ from measurements of the tangential components $\mathbf{n}\times\mathbf{H}$ and $\mathbf{n}\times\mathbf{E}$ of the fields on some surface Γ (with normal $\mathbf{n}$) enclosing the region Ω where the material parameters are unknown. Uniqueness of the solution for this inverse boundary value problem has been proved, provided ω is not a resonant frequency [23]. For the moment we take $\mathbf{J}_s = 0$ assuming the sources are included in the boundary conditions. It is worth noticing that in the sensing coil the measurements of induced voltage can be expressed as line integral of the tangential component of $\mathbf{E}$ along the coil. It can also be described as surface integral of the normal component of the rate of change of magnetic flux density $\mathbf{B}$. Fig. 1 shows the general form of MIT measurement with sensing and excitation coils.

The methodology for establishing the derivative of the boundary measurements with respect to a perturbation of a material parameter was established in the fundamental paper of Calderón [2] for the static case $\omega = 0$. The general case for time harmonic Maxwell's equations was treated by [33]. These results require some slight modification for application to MIT. In this case, we are not measuring on an isolated boundary. Typically we have an arrangement of coils on some surface Γ but boundary conditions (such as screening by a conductive or magnetic shield) are applied on some surface containing this. We can think of an idealized excitation coil as imposing a predetermined tangential component of $\mathbf{H}$ on Γ, and our idealized measurement as an integral of $\mathbf{E}$ around an infinitesimal loop on Γ. This is no worse than the idealization in the low frequency case (EIT) that one can apply arbitrary current patterns to the surface and measure the voltage everywhere.

In practice we measure a finite subset of the idealized data, but it is important to know at least that if we collected ideal data then the material parameters are uniquely determined. This question, called *uniqueness of solution* by mathematicians, is the practical question of *sufficiency of data* for the engineer. The measurement arrangements of MIT using a system of coils does not fit exactly in to this formalism, meaning that the measurement can not be done at all points surrounding the object. There is no barrier to electric and magnetic fields on the surface containing the coils so we must model them by a current source term $\mathbf{J}_s$, and impose boundary conditions on some larger enclosing surface. We will address this in the next section. For the moment, our ideal data is the transfer impedance on the surface Γ, where we have complete control of the tangential component of $\mathbf{H}$ and knowledge of the transfer impedance of $\mathbf{E}$ (or vice versa). There is of course a parallel impedance due to the region exterior to Γ, which we will assume is known by calibration and has already been subtracted.

It is convenient to recast the data on Γ in an integral of the normal component of the vector field $\mathbf{E}\times\mathbf{H}$. Taking the electric and magnetic fields from two different excitations, gives fields $\mathbf{E}_i, \mathbf{H}_i$, $i = 1, 2$. Assuming the magnetic field on Γ to be prescribed and the tangential electric field to be measured, a perturbation in the material parameters gives rise to perturbed fields, and a perturbed

measurement

$$\int_{\Gamma} \mathbf{H}_2 \times \delta\mathbf{E}_1 \cdot \mathbf{n}\, \mathrm{d}\mathbf{x}^2 = \int_{\Omega} -\mathrm{i}\omega\delta\mu\mathbf{H}_1 \cdot \mathbf{H}_2 + (\delta\sigma + \mathrm{i}\omega\delta\varepsilon)\mathbf{E}_1 \cdot \mathbf{E}_2 \, \mathrm{d}\mathbf{x}^3 + O(\|(\delta\sigma, \delta\mu, \delta\varepsilon)\|^2) \tag{3}$$

A rigorous derivation of this formula appears in [33] and and informal derivation for example in [6]. Taking $\mathbf{H}_2$ to be the field due to the excitation of measurement coil 2 (but idealized as a flux over the surface Γ) with a unit current, this reduces to δV_{21} the change of the induced voltage on the measurement coil 2 when coil 1 is excited. The difficulty with this derivation is that the both measurement and excitation coils are idealized as loops on a surface Γ, and the magnetic field must be assumed zero on portions of Γ that are not excited. This clearly does not accurately model the situation in MIT.

Although one could in principle calculate the sensitivity using a numerical solver for Maxwell's equations by successively making small perturbations to voxels in the model, this would result in a large number of field solutions, whereas calculation using the above formula, effectively an 'adjoint field method' requires only one $\mathbf{E}$ and $\mathbf{H}$ solution for each drive and measurement coil. In the next section we derive the sensitivity formula for the case where discrete coils are used in the interior of the domain, and the eddy current approximation to Maxwell's equations is used.

2.2 Coil Model and Sensitivity

There are a number of ways to model the excitation and measurement coils. As in EIT where the conductive electrodes must be modeled, the presence of the coils can affect the fields. Rather than modeling individual turns of copper wire, we will use a simplified model of a coil as a surface, (topologically at least) an open ended cylinder. When used as an excitation coil this surface carries a tangential current $\mathbf{J}_s$. This is equivalent to a surface that is perfectly conducting in one direction (angular for a cylinder) and an insulator in another (axial) direction, with each loop fed by a perfect current source.

A typical arrangement of the sensors for MIT uses fixed excitation and the measurement coils. There might be an external screen modeled as an electrical conductor, which means that the tangential component of $\mathbf{E}$ vanishes. Where shielding is not possible one would nevertheless need to apply far field boundary conditions to Maxwell's equations. It is important to note that the electromagnetic fields inside the sensor area and between the coils and the shield are coupled so that we can no longer apply the approximation that measurement is made on a surface, which decouples the problem. Instead we apply the boundary condition $\mathbf{n} \times \mathbf{E} = 0$ on the shield Γ, and include source terms $\mathbf{J}_s$ for the coils as above.

In areas (such as the air gap surrounding the coils) the same approximation, that of ignoring the displacement current, results in the magnetostatic approximation $\nabla \times \mathbf{H} = 0$. This does not allow wave propagation effects and is valid provided our system is small compared with the wavelength

of electromagnetic waves in air. Our coils are considered as electro-magnets not radio transmitting antennas. Combining (1) and (2) we obtain

$$\nabla \times \left(\frac{1}{\mu} \nabla \times \mathbf{E} \right) + \mathrm{i}\omega\xi\mathbf{E} = -\mathrm{i}\omega\mathbf{J}_s \tag{4}$$

Where ξ is the complex admittivity $\xi = \sigma + \mathrm{i}\omega\varepsilon$. We now consider the case where we excite one coil. Suppose that the admittivity is perturbed $\xi \to \xi + \delta\xi$ with the resulting change in the field $\mathbf{E} \to \mathbf{E} + \delta\mathbf{E}$ while the current $\mathbf{J}_s$ is held constant. Our aim is to find the linearized change in the voltage measured on some other coil, so in this derivation we will neglect second and higher order terms. In this section we pay special attention to boundary conditions. Many authors in NDT and medical imaging have derived, with varying degrees of rigor a similar formula where the sensitivity of a measurement to a local change in conductivity is given by the inner product of the electric fields from two coils. Others use an experimentally determined sensitivity [19] or a perturbation of a finite element model. Indeed [33] provides a rigorous derivation for the the inverse boundary value problem for Maxwell's equations. We feel a more careful explanation is required for the eddy current approximation to Maxwell's equations with coil measurements. Indeed there is some confusion in the literature, for example [17] quotes the sensitivity as the inner product of magnetic fields. The result of our derivation is that as long as the domain is electrically shielded, or we impose vanishing boundary conditions at infinity the usual sensitivity formula holds. However the result must be used with caution when there are other boundary conditions as this will result effectively in missing boundary data. A more detailed derivation along the lines of Calderón [2] would prove that we have calculated the Fréchet derivative (rather than simply the Gâteaux derivative) in suitable normed spaces. Applying (4) to $\mathbf{E}$ and $\mathbf{E} + \delta\mathbf{E}$, then subtracting and neglecting higher order terms gives

$$\nabla \times \left(\frac{1}{\mu} \nabla \times \delta\mathbf{E} \right) + \mathrm{i}\omega(\delta\xi\mathbf{E} + \xi\delta\mathbf{E}) = 0. \tag{5}$$

Taking the dot product with $\mathbf{E}$ yields

$$\frac{1}{\mu}\mathbf{E} \cdot \nabla \times (\nabla \times \delta\mathbf{E}) + \mathrm{i}\omega\delta\xi\mathbf{E} \cdot \mathbf{E} + \mathrm{i}\omega\xi\mathbf{E} \cdot \delta\mathbf{E} = 0 \tag{6}$$

from which we seek to remove the term in $\delta\mathbf{E}$ (in the interior). We use the identity

$$\nabla \cdot (\mathbf{E} \times \nabla \times \delta\mathbf{E}) = \mathbf{E} \cdot \nabla \times \nabla \times \delta\mathbf{E} - (\nabla \times \mathbf{E}) \cdot (\nabla \times \delta\mathbf{E}) \tag{7}$$

and its counterpart with $\mathbf{E}$ and $\delta\mathbf{E}$ reversed

$$\begin{aligned} \nabla \cdot (\delta\mathbf{E} \times \nabla \times \mathbf{E}) &= \delta\mathbf{E} \cdot \nabla \times \nabla \times \mathbf{E} - (\nabla \times \delta\mathbf{E}) \cdot (\nabla \times \mathbf{E}) \\ &= -\mathrm{i}\omega\mu\xi\delta\mathbf{E} \cdot \mathbf{E} - \mathrm{i}\omega\mu\delta\mathbf{E} \cdot \mathbf{J}_s - (\nabla \times \delta\mathbf{E}) \cdot (\nabla \times \mathbf{E}) \end{aligned} \tag{8}$$

using (4). Subtracting (8) from (7) gives

$$\begin{aligned}\nabla\cdot(\mathbf{E}\times\nabla\times\delta\mathbf{E}-\delta\mathbf{E}\times\nabla\times\mathbf{E}) = \mathbf{E}\cdot\nabla\times\nabla\times\delta\mathbf{E}\\ +\mathrm{i}\omega\mu\xi\mathbf{E}\cdot\delta\mathbf{E}+\mathrm{i}\omega\mu\delta\mathbf{E}\cdot\mathbf{J}_s\end{aligned} \tag{9}$$

eliminating the $\delta\mathbf{E}$ terms using (6) then integrating over the domain and using Gauss' theorem, together with the vanishing of the tangential components of $\mathbf{E}$ and $\delta\mathbf{E}$ on Γ finally gives

$$\int_\Omega \delta\mathbf{E}\cdot\mathbf{J}_s\,\mathrm{d}\mathbf{x}^3 = \int_\Omega \delta\xi\,\mathbf{E}\cdot\mathbf{E}\,\mathrm{d}\mathbf{x}^3 \tag{10}$$

One can calculate the sensitivity of a voltage measured on coil 2 when coil 1 is excited. Notice that the left hand side of (10) is a volume integral and this requires a word of explanation. If the coils are thin they can be modelled by a current density that is a surface measure reducing the left hand side to a surface integral. Coils with large number of turns can be modelled by a solid annulus and $\mathbf{J}_s$ in the direction of the turns. Clearly $\mathbf{J}_s$ vanishes off the coils.

$$\int_\Omega \delta\mathbf{E}_1\cdot\mathbf{J}_{s2}\;\mathrm{d}\mathbf{x}^3 = \int_\Omega \delta\xi\,\mathbf{E}_1\cdot\mathbf{E}_2\;\mathrm{d}\mathbf{x}^3 \tag{11}$$

The left hand side here is now the change in voltage induced on our ideal coil provided a unit current is driven in coil 2. It must be emphasized that with non-zero (for example impedance) boundary conditions on the shield Γ the sensitivity would involve boundary terms that are unknown. Alternatively one could assume that the domain of interest extends to infinity and the fields decay to zero

3 Simulated MIT system

In this paper a simulated MIT system has been used to generate the data for image reconstruction. The simulated system has eight coils used for excitation and sensing. The coils have 0.04 m inner and 0.05 m outer diameter and 0.02 m length and they are arranged in a horizontal circular ring surrounding the object to be imaged. In this example the distance between the center of two coils on opposite sides is 0.160 m, the center of the coils ring is at $(0,0,0)$. Fig. 2 shows the coil arrangement of this virtual MIT system. The system could have an external magnetic shield or electrostatic shields, but in this paper the far field boundary condition $\mathbf{B}\cdot\mathbf{n}=0$ is applied on an external surface and a shield has not been incorporated. An efficient alternative way to apply far field conditions would be to use perfectly matched Layers [14]. All voltages are normalized with respect to the free space induced voltage and a $1\mathrm{Am}^{-2}$ current is applied to the excitation coil for simplicity. The region of interest for imaging is a vertical cylinder with radius 7.6 cm, length 6 cm centered at $(0,0,0)$, which we will refer to as C1. Each coil is excited in turn and the induced voltages are measured in the remaining coils giving 7x8/2=28 linearly independent trans-impedance

measurements as data. The real part of the induced voltage (in phase to the excitation current) has been used for the conductivity reconstruction. The model used in this study is simplified but it has all essential components of an inverse eddy current problem. Of course work is underway in several groups to design MIT systems optimized for applications in medical diagnosis, but such work is beyond scope of this paper.

4 Forward problem

The purpose of the forward solver in MIT is to predict the measurement given the geometry, material distribution and the excitation currents. As we shall see in the next section one needs to calculate the interior electric and magnetic fields to be able to efficiently calculate the Jacobian matrix. Commercial FEM packages typically provide insufficient access to data structures representing the system matrices and shape functions necessary for the efficient implementation of the inverse solver. Also they are not optimized for repeated calculations with small variations in material parameters. For these reasons we implemented our own forward solver tightly integrated with the solution to the inverse problem. The electromagnetic field in the eddy current problem can be described either in terms of a field, a potential or a combination of both. One can use various combinations of these quantities as state variables [1]. Although different formulations would produce the same answers in exact arithmetic, they may differ in accuracy when implemented numerically and the implementation will differ in complexity and computational cost. We use a formulation based on magnetic vector potential and electric scalar potential, the so called $\mathbf{A},\mathbf{A}$-V [1]. We use first order tetrahedral edge finite element for the magnetic vector and the first order nodal tetrahedral elements electric scalar potential. For the field quantities we have $\mathbf{E} = -\mathrm{i}\omega(\mathbf{A} + \nabla V)$ (the time derivative of the electric potential is used to ensure the symmetry of Galerkin equations) and $\mathbf{B} = \nabla \times \mathbf{A}$. Let us consider the quasi-static electromagnetic fields governed by

$$\nabla \times \left(\tfrac{1}{\mu}\nabla \times \mathbf{A}\right) + \mathrm{i}\omega\xi(\mathbf{A} + \nabla V) = \mathbf{J_s}. \tag{12}$$

$$\mathrm{i}\omega\nabla \cdot (\xi(\mathbf{A} + \nabla V)) = 0 \tag{13}$$

Far field boundary conditions are set with the normal component of magnetic flux density zero on the surface of the whole simulation domain Γ and $\mathbf{n} \cdot (\mathrm{i}\omega\xi\mathbf{A} + \mathrm{i}\omega\xi\nabla V) = 0$ on Γ_d, the surface of the eddy current region.

In edge FEM on a tetrahedral mesh, a vector field is represented using a basis of vector valued functions $\mathbf{N}_{ij}$ associated with the edge between nodes i and j

$$\mathbf{N}_{ij} = L_i \nabla L_j - L_j \nabla L_i. \tag{14}$$

where L_i is a nodal shape function. We define an electric vector potential $\mathbf{T}_s$ in the coil region to represent the current in the excitation coil such that $\nabla \times \mathbf{T}_s = \mathbf{J}_s$. Using this formulation guarantees a divergence free current source for the right hand side of equation (12) and improves the

convergence of the linear solver. For simple coil shapes we use an analytical formulation for the computation of $\mathbf{T}_s$ [1], and there is no need to mesh the coil itself. For complicated coil shapes we can solve boundary value problem $\nabla \times \left(\frac{1}{\sigma}\nabla \times \mathbf{T}_s\right) = 0$ with suitable boundary conditions in the coil region.

Galerkin's approximation using edge element basis functions yields

$$\int_{\Omega} (\nabla \times \mathbf{N}\frac{1}{\mu} \cdot \nabla \times \mathbf{A})\, \mathrm{d}\mathbf{x}^3 + \int_{\Omega_d} (\mathrm{i}\omega\xi\mathbf{N} \cdot (\mathbf{A} + \nabla V))\, \mathrm{d}\mathbf{x}^3 = \int_{\Omega_c} (\nabla \times \mathbf{N} \cdot \mathbf{T}_s)\, \mathrm{d}\mathbf{x}^3 \tag{15}$$

and

$$\int_{\Omega_d} (\mathrm{i}\omega\xi\nabla L \cdot (\mathbf{A} + \nabla V))\, \mathrm{d}\mathbf{x}^3 = 0. \tag{16}$$

where $\mathbf{N}$ is any linear combination of edge basis functions, Ω is the entire region, Ω_d the eddy current region, and Ω_c the current source region. The linear system of equations can be solved using the Incomplete Cholesky Conjugate Gradient (ICCG) method [1]. The induced voltages (V_m) in sensing coils are calculated using

$$V_m = -\mathrm{i}\int_{\Omega_c} (\mathbf{A} \cdot \mathbf{J}_0)\, \mathrm{d}\mathbf{x}^3 \tag{17}$$

where $\mathbf{J}_0$ is a virtual unit current density passing through the coil.

5 Sensitivity analysis

Each row of the Jacobian is derived from the solution to two forward problems: an ordinary and an "adjoint" problem. In contrast, a perturbation computation of the Jacobian (that is a finite difference approximation to the Fréchet derivative) requires the solution of multiple forward problems. For each driven coil the forward problem must be solved for a perturbation in each unknown parameter used in modeling the unknown region. With the $\mathbf{A}, \mathbf{A}$-V formulation and using the edge FEM, the sensitivity to a change in the conductivity of the conducting region can be calculated using an adjoint field method as derived in this paper and discussed in [6], [8], [12] where the integral becomes the inner product of $\mathbf{E}$ fields and the Jacobian can be calculated by performing this integration for a chosen basis for the conductivity perturbation $\delta\sigma$. Using the shape function of edge elements $\{\mathbf{N}_e\}$ and nodal elements of L_e, the electric field $\mathbf{E}$ in each point inside each element can be expressed as follows

$$\mathbf{E} = -\mathrm{i}\omega(\{\mathbf{N}_e\mathbf{A}_e\} + \nabla L_e V_e) \tag{18}$$

where $\{\mathbf{A}_e\}$ are defined along the edges, and V_e is the calculated electric potential (time derivative of the electric potential) for the nodes. The sensitivity of the i, j measurement to a change in the conductivity in the kth element is then

$$S = \frac{\partial V_{ij}}{\partial \sigma_k} = -\frac{\omega^2}{I_i I_j} \left(\int_{\Omega_k} (\{\mathbf{A}_e^i \mathbf{N}_e + V_e^i \nabla L_e\} \cdot \{\mathbf{N_e} \mathbf{A}_e^j + \nabla L_e V_e^j\}^T) \, \mathrm{d}\mathbf{x}^3 \right) \tag{19}$$

where Ω_k is the interior of the k-th element, I_i and I_j are the excitation currents in coils i and j respectively.

In the edge FEM software implemented here, one can calculate $\mathbf{E}$ in all elements by (18) where $\{\mathbf{N}_e\}$ is a matrix of shape functions for all elements and $\{\mathbf{A}_e\}, V_e$ are the solution of the forward problem. Equation (19) applies also to a region Ω_f that is a union of elements. Then the computation of the Jacobian matrix is matrix vector multiplication for each measurement.

The sensitivity calculated in (19) is a complex number $S = S_r + \mathrm{i}S_i$ where S_r, S_i are real and imaginary parts of the sensitivity. These terms represent the change in V_r, V_i, i.e. real and imaginary parts of the measured voltage $V = V_r + \mathrm{i}V_i$. Some medical MIT measurement systems [15] measure the phase ϕ. The sensitivity with respect to the phase is calculated as follows

$$S_\phi = \frac{\partial \phi}{\partial \sigma} = \frac{V_r S_i - V_i S_r}{|V|^2}. \tag{20}$$

5.1 Jacobian matrix

Linear reconstruction relies on the assumption that for small changes, the induced voltages can be approximated in a linear fashion with the conductivity, which may be expressed using the Jacobian matrix $\mathbf{J}$ as

$$\mathbf{F}(\sigma) - \mathbf{V}_m = \mathbf{J}(\sigma - \sigma_{\text{true}}) + O(\|\sigma - \sigma_{\text{true}}\|^2) \tag{21}$$

where $\mathbf{V}_m$ is the measurement data (due to the conductivity distribution σ_{true}) and $\mathbf{F}$ is the forward operator that maps the conductivity to the measurement data. A powerful set of techniques for exploring sets of equations or matrices that are either singular or numerically very close to singular is Singular Value Decomposition (SVD). The SVD allows one to diagnose rank deficiency in a given matrix, and shows how many unknowns one can expect to recover reliably with a given data precision.

To illustrate the degree of ill conditioning in the problem we have plotted the singular values on a logarithmic scale (Fig. 3). The roughly linear decay of the first 28 singular values shows that the problem is severely ill posed. In a noise and error free situation it is possible to reconstruct an image with up to 28 parameters. In real data and with measurement errors, including the image reconstruction components of singular vectors with small singular values may not be justified. It

is worth noticing that some of these small singular values may represent important and desirable parts of the images which may not be reconstructed due to noise and error in the measurement.

6 Image reconstruction

The image reconstruction problem is to find the distribution of electrical conductivity σ within the region of interest using a knowledge of all 28 measurements of induced voltage. This can be done using iterative schemes based on optimization methods. However the inverse problem is ill posed, and any discrete linearized approximation will be ill-conditioned as we have seen. Moreover the voltage data will be contaminated with measurement error.

To overcome this problem we include *a priori* information to regularize the ill posed problem. A natural assumption is that $\|\mathbf{R}(\sigma-\sigma_{\text{ref}})\|$ is not too large where σ_{ref} is an *a priori* guess for the conductivity distribution. This approach is called generalized Tikhonov regularization and the matrix $\mathbf{R}$ is typically a difference operator between neighboring voxels. This corresponds statistically to assuming a correlation between neighboring voxel values. We take $\mathbf{R}$ to be a discrete difference approximation to the Laplacian operator. Specifically $R_{ij}=-1$ for $i\neq j$ when two elements are neighbors (sharing at least one node) and $R_{ii}=-\Sigma_{j:j\neq i}R_{ij}$.

The regularized inverse problem is now a problem in optimization: to find σ that minimizes the function $g(\sigma)$ defined by

$$g(\sigma)=\|\mathbf{F}(\sigma)-\mathbf{V}_m\|^2+\alpha^2\|\mathbf{R}(\sigma-\sigma_{\text{ref}})\|^2. \tag{22}$$

We apply the iterative Gauss-Newton method to solve this problem. The descent direction for σ is given by

$$\begin{aligned}\delta\sigma_n=-(\mathbf{J}_n^T\mathbf{J}_n+\alpha^2\mathbf{R}^T\mathbf{R})^{-1}(\mathbf{J}_n^T(\mathbf{F}(\sigma_n)-\mathbf{V}_m)\\ +\alpha^2\mathbf{R}^T\mathbf{R}(\sigma_n-\sigma_{\text{ref}}))\end{aligned} \tag{23}$$

where n is the iteration step, for $n=1$ this is a linear reconstruction algorithm. Here $\mathbf{J}_n$ is the Jacobian calculated with the conductivity σ_n. The regularization matrix $\mathbf{R}$ with a suitable regularization parameter α penalizes extreme changes in conductivity, removing the instability in the reconstruction, at the cost of producing artificially smooth images. The regularization parameter should yield a suitable balance between two terms of equation (22). Unfortunately there is no reliable method to choose the regularization parameter for nonlinear image reconstruction. In this study we choose the regularization parameter empirically, our chosen value is $\alpha=10^{-10}=1.6\times10^{-4}\|\mathbf{J}\|/\|\mathbf{R}\|$ (where $\mathbf{J}$ the first Jacobian) for all iteration steps.

As an iterative reconstruction algorithm the regularized Gauss-Newton method starts with an initial conductivity distribution, by default σ_{ref}. The forward problem is solved and the predicted voltages compared with the calculated voltages from the forward model. The conductivity is then updated using (23). The process is repeated until the predicted voltages from the finite element

method agree with the calculated voltages from the finite element model to measurement precision. The Jacobian matrix is also updated at each step. If the solution of the inverse problem is close to the initial guess the method typically converges. To avoid local minima, especially when the initial guess is far from the true solution, we need to define a step length λ that sufficiently reduces the objective function and satisfies the Wolf condition [21] that $g(\sigma_{n+1})$ satisfies the inequality

$$g(\sigma_{n+1}) \leq g(\sigma_n) - 10^{-3}\lambda \mathbf{J}^T(\sigma_n)[\mathbf{F}(\sigma_n) - V_m]^T \delta\sigma \tag{24}$$

and we use the update $\sigma_{n+1} = \sigma_n + \lambda\delta\sigma_n$. To find λ we use the bisection method [7]. The iteration is terminated using Morozov's criterion: when the residual error falls below the measurement accuracy.

6.1 Results and discussion

The simulated phantom consists of a region of interest for the image with a cylinder of diameter 15.2 cm and length of 6 cm centered at (0,0,0) cm, (this is the cylinder previously named C1) with a background conductivity of 0.2 S/m. The frequency of the excitation signal is 10 MHZ in all examples. In all cases, 2 percent Gaussian noise (2 percent of the maximum voltage) was added to the simulated data. Measured data were generated in a 208000 tetrahedral elements mesh (C1 includes 25670 elements). The inverse problem has been solved in a coarser mesh of total 65603 elements where the region of interest for imaging includes 2875 elements (C1 region in inverse mesh). It is worth noticing that to solve the forward problem the whole region including conductive region and free space in Fig. 1 needs to be meshed. The inverse problem is only solved in conductive region, which includes a much smaller number of tetrahedral elements. In addition the regularization couples the values of nearby elements, smoothing the solution and further reducing the effective number of degrees freedom in the reconstructed image.

The computer used for simulation had a 1.7 GHz Intel Pentium M processor and 512 MB of RAM. The computational time for each nonlinear iteration of the inverse problem (consisting mainly of the forward solver, Jacobian calculation and inversion) was 53 minutes. The major part of the computational time includes solving two linear system of equations: one is for the forward problem involving a large but sparse matrix and the other one involves solution of a smaller but full matrix arising from the inverse problem.

In the first example (Fig. 4), a cylinder of diameter of 4 cm with conductivity of 1.4 S/m, one linear step has been used to reconstruct the single object. Although the the absolute conductivity values are not recovered accurately the location and the size of the object was recovered. Fig. 5 shows two inclusions with conductivity of 0.8 S/m, the linear reconstruction has been shown in Fig. 5.b, the center of the recovered inclusion is slightly shifted towards the boundary and the absolute values are incorrect. By using 5 steps of the nonlinear reconstruction the location of inclusions and the range of the conductivity values are recovered with reasonable accuracy. Fig. 6 exhibits higher contrast conductivity inclusions with conductivity of 0.01 S/m. A linear reconstruction has been shown in Fig. 6.b and after 9 steps the absolute values and the locations are in good agreement

with the true image. Fig 7 shows multiple inclusions that can not be recovered in first iteration; in the 5th iteration a satisfactory image has been produced. The last example (Fig. 8) is adding an object at the center of the image in Fig. 7. In the first iteration step the background has a homogenous conductivity of 0.2 S/m and the sensitivity analysis (for two opposite coils) shows that the sensitivity valuse are larger near to the boundary and smaller at the center as previously demonstrated in [27]. After the first iteration the Jacobian is updated, and as it can be seen in Fig. 9 the sensitivity map now has larger values at the center compared to the sensitivity of the homogenous background. After 5 iteration steps all five inclusions could be reconstructed(Fig 8.c). The reduction of 28 voltage differences can be seen in Fig. 10.a and reduction of cost function (of equation 22) has been shown in Fig. 10.b. In order to show how the image quality is changing during the iteration steps we define image quality with respect to the true conductivity $||\sigma_n - \sigma_{true}||/||\sigma_{\text{true}}||$ (where σ_n is a vector including the conductivity of all voxles in iteration number n and σ_{true} is the vector including all true conductivities) and it can be seen in Fig. 10.c that the image quality is improved by the iteration steps.

7 Conclusions

We presented an edge based finite element method for the forward problem, a sensitivity formula to calculate the changes in induced voltages due to a small change in the conductivity of a region, and an image reconstruction scheme for MIT. The image reconstruction method has been tested on various examples with conductivity ranges encountered in medical applications. Although a linear approximation may work for some simple conductivity distributions the general case requires a nonlinear approach. This paper demonstrates the advantages of nonlinear method both in terms of locating of inclusions and reconstruction of the absolute conductivity values. It is clear from this work that a nonlinear algorithm including an updated forward model and recalculated Jacobian offers improvements over equivalent linear reconstructions with simulated data. However the application of this method to *in vitro* or *in vivo* experimental biomedical data requires a sufficiently accurate measurement system and forward model to justify the computational effort. If a linear algorithm fits the measured data to within the precision of measurement and model a non-linear algorithm is unlikely to offer any improvement. In an industrial setting, with fixed and simple geometry and large conductivity contrasts, we have already demonstrated that non-linear reconstruction is worthwhile for experimental data [32]. In [32] paper we considered high conductivity of metal objects relevant to industrial tomography problems. In the low contrasts typical of medical problems treated in this paper better absolute reconstruction could be obtained. The application to experimental data from biomedical problems is the subject of our continuing efforts.

Acknowledgements

The authors would like to thank the EPSRC for supporting this work with grant GR/R64278/01. We would also like to acknowledge the contribution of Professor Tony Peyton and his colleagues who introduced us to (industrial) MIT, and to Corus UK Ltd - R,D&T. Teesside Technology Center for their support. We would also like to thank Professor Alain Bossavit for helpful and inspiring discussions on computational electromagnetics, and the anonymous referees for their many helpful suggestions.

References

[1] O. Biro, "Edge element formulations of eddy current problems", *Computer methods in applied mechanics and engineering*, 169 (1999), pp. 391-405, 1999.

[2] A. P. Calderón, "On an inverse boundary value problem", *Seminar on Numerical Analysis and its Applications to Continuum Physics* , pp. 65-73, Soc. Brasil. Mat., Rio de Janeiro,, 1980.

[3] R. Casanova, A. Silva and A. R. Borges, "MIT image reconstruction based on edge-preserving regularization", *Physiol. Meas.*, 25, pp. 195-207, 2004.

[4] H. Dehghani, B. W. Pogue, J. Shudong, B. Brooksby and K. D. Paulsen, "Three-Dimensional Optical Tomography: Resolution in Small-Object Imaging", *Applied Optics*, Volume 42, pp. 3117-3128, June 2003.

[5] R. Casañas, H. Scharfetter, A. Altes, A. Remacha, P. Sarda, J. Sierra, R. Merwa, K. Hollaus and J. Rosell, "Measurement of liver iron overload by magnetic induction using a planar gradiometer: preliminary human results", *Physiol. Meas.*, 25, pp. 315-323, 2004.

[6] D. N. Dyck, D. A. Lowther and E. F. Freeman, "A Method of computing the sensitivity of the electromagnetic quantities to changes in the material and sources", *IEEE Trans. Mag.*, vol. 3, no. 5, pp. 3415-3418, 1994

[7] P.C. Hansen, *Rank-Deficient and Discrete Ill-Posed Inverse Problems*, SIAM, Philadelphia, PA, 1998.

[8] H. Huang, T. Takagi and H. Fukutomi, "Fast signal predictions of noised signals in eddy current testing", *IEEE Trans. on Mag.*, vol. 36, Issue. 4, Part. 1, pp. 1719-1723, 2000.

[9] N. G. Gencer and M. N. Tek,"Electrical conductivity imaging via contactless measurements", *IEEE Trans. on Medical Imaging*, vol. 18, Issue. 7, pp. 617-627, 1999.

[10] H. Griffiths, W. R. Stewart and W. Gough, "Magnetic induction tomography: Measurements with a single channel", *X-ICEBI*, Barcelona, pp. 361-364, 1998.

[11] H. Griffiths, “Magnetic induction tomography”, *Measurement Science and Technology*, 12, 8, pp. 1126-1131, 2001.

[12] K. Hollaus, C. Magele, R. Merwa and H. Scharfetter, “Fast calculation of the sensitivity matrix in magnetic induction tomography by tetrahedral edge finite elements and the reciprocity theorem”, *Physiol. Meas.*, 25, pp. 159-168, 2004.

[13] K. Hollhaus, C. Magele, B. Brandstätter, R. Merwa and and H. Scharfetter, “Numerical simulation of the forward problem in magnetic induction tomography of biological tissue”, In *Proc. 10th IGTE Symposium*, pp. 381-384, 2002.

[14] S. Järvenpää, “Implementation of PML absorbing boundary condition for solving Maxwell’s equations with Whitney elements”. PhD. Dissertation, Research Reports A35, Rolf Nevanlinna Institute, Helsinki, 2001.

[15] A. Korjenevsky, V. Cherepenin and S. Sapetsky, “Magnetic induction tomography: experimental realization”, *Physiol. Meas.*, v. 21(1), pp. 89-94, 2000.

[16] Y. Li, L. Udpa and S. S. Udpa, “ Three-Dimensional Defect Reconstruction From Eddy-Current NDE Signals Using a Genetic Local Search Algorithm”, *IEEE Trans. Mag.*, vol. 40, no. 2, pp. 410-417, 2004.

[17] C. Ktistis, R.O. Mackin, H.S. Tapp, and A.J. Peyton “Initial experimental results from an electromagnetic induction tomography system with low conductivity materials”, Proc 4th World Congress on Industrial Process Tomography, Aizu, Japan, 2005.

[18] W.R.B. Lionheart, N. Polydorides, A. Borsic, “The Reconstruction Problem”, in *Electrical Impedance Tomography: Methods, History and Applications*, (ed) D S Holder, Institute of Physics, pp. 3-64, 2004.

[19] X. Ma, A. J. Peyton, R. Binns, and S. R. Higson, Electromagnetic Techniques for Imaging the Cross-Section Distribution of Molten Steel Flow in the Continuous Casting Nozzle, IEEE Sensors J . 5, 224-232, 2005.

[20] R. Merwa, K. Hollhaus, B. Brandstätter and H. Scharfetter, “Numerical solution of the general 3D eddy current problem for magnetic induction tomography (spectroscopy)”, *Physiol. Meas.* . Volume 24, Number 2, pp. 545-554, 2003.

[21] J. Nocedal and S. J. Wright, “ Numerical Optimisation”, *Springer Series in Operational Research*, Springer, Berlin, 1999.

[22] S. J. Norton and J. R. Bowler “Theory of eddy current inversion”, *Journal of Applied Physics*, Vol 73(2) pp. 501-512, January 15, 1993.

[23] P. Ola, E. Päivärinta, E. Somersalo, “An inverse boundary value problem in electrodynamics”, *Duke Math. J.* 70 pp. 617-653, 1993.

[24] A. J. Peyton, Z. Z. Yu, S. Al-Zeibak, N. H. Saunders and A. R. Borges, “Electromagnetic imaging using mutual inductance tomography: Potential for process applications”, *Part. Syst. Charact.*, vol.12, pp. 68-74, 1995.

[25] N. Polydorides and W. R. B. Lionheart, “A MATLAB toolkit for three dimensional electrical impedance tomography: A contribution to the EIDORS project”, *Meas Sci Tech*, vol. 13, no. 12, pp. 1871-1883, 2002.

[26] J. Rosell, R. Casañas and H. Scharfetter, “Sensitivity maps and system requirements for Magnetic Induction Tomography using a planar gradiometer”, *Physiol. Meas.* 22, pp. 121-130, 2001.

[27] H. Scharfetter, P. Riu, M. Populo and J. Rosell, “Sensitivity maps for low-contrast-perturbations within conducting background in magnetic induction tomography (MIT)”, *Physiol Meas*, 23, pp. 195-202, 2002.

[28] H. Scharfetter, T. Schlager, R. Stollberger, R. Felsberger, H. Hutten and H. Hinghofer-Szalkay, “Assessing abdominal fatness with local bioimpedance analysis: Basics and experimental findings”, *Int J Obes Relat Metab Disord.*, 25, pp. 502-511, 2001.

[29] H. Scharfetter, R. Casañas and J. Rosell, “Biological Tissue Characterization by Magnetic Induction Spectroscopy (MIS): Requirements and Limitations”, *IEEE Transactions on Biomedical Engineering*, Vol. 50, No. 7, 2003.

[30] M. Soleimani, W. R. B Lionheart, C. H. Riedel and O. Dossel, “Forward Problem in 3D Magnetic Induction Tomography (MIT)”, in *Proc. 3rd World Congress on Industrial Process Tomography*, Banff Canada, pp. 275-280, 2003.

[31] M. Soleimani and W. R. B. Lionheart, “ Image Reconstruction in Three-Dimensional Magnetostatic Permeability Tomography”, IEEE Trans. Mag, 41, pp. 1274-1297, 2005

[32] M. Soleimani, W. R. B. Lionheart, AJ Peyton, X. Ma and S.R. Higson, “A 3D inverse finite element method applied to experimental eddy current imaging data”, *IEEE Trans Magnetics*, Vol. 42, No. 5, pp. 1560-1567, May 2006.

[33] E. Somersalo, D. Isaacson and M. Cheney, “A linearized inverse boundary-value problem for Maxwell equation”, *J Comp. Appl. Math.* 42, pp. 123-136, 1992.

[34] T. Takagi, H. Huang, H. Fukutomi and J. Tani , “Numerical Evaluation of Correlation between Crack Size and Eddy Current Testing Signals by a Very Fast Simulator”, *IEEE Trans. MAG.*, vol. 34, no. 5, pp. 2581-2584, 1998.

List of Figures

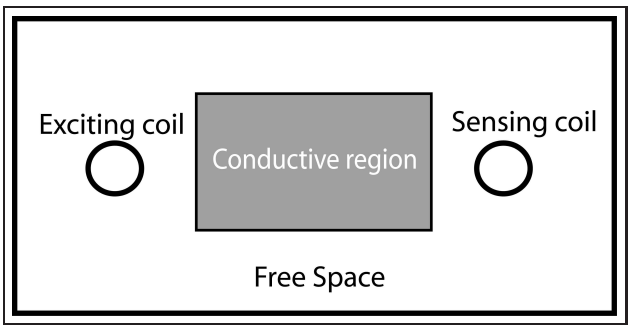

Figure 1: Overview of an eddy current problem.

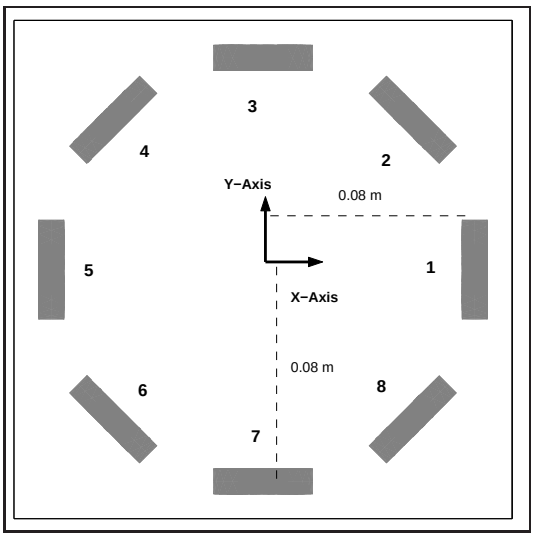

Figure 2: Excitation and sensing coils, view from top

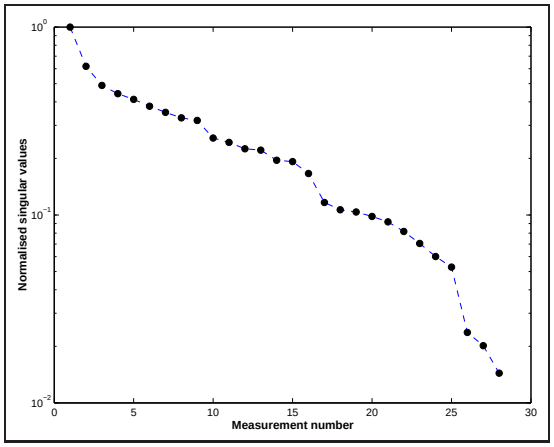

Figure 3: Singular values of the Jacobian matrix (**J**) for the real part of the measurement voltages on a logarithmic scale.

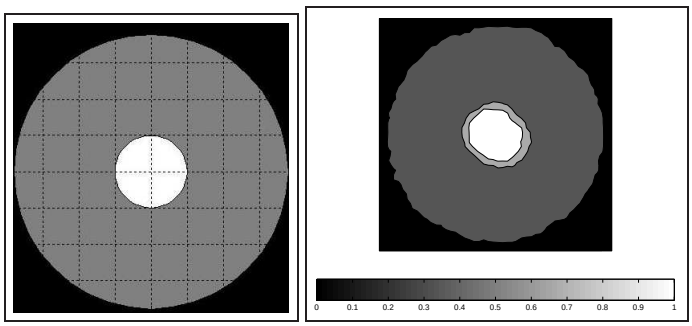

(a) (b)

Figure 4: (a): One inclusion at the center, a cylinder of diameter of 4 cm with conductivity of 1.4 S/m, and (b) Reconstructed image using a single step

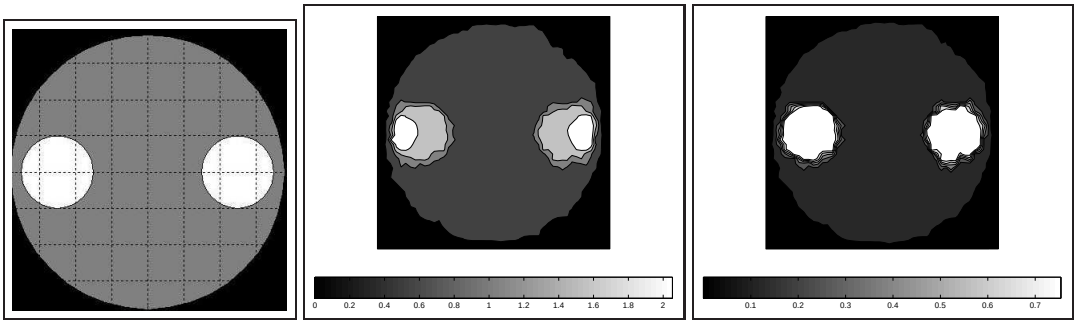

(a) (b) (c)

Figure 5: (a): Two inclusions with diameter of 4 cm with conductivity of 0.8 S/m centered at (-5,0,0) cm and (5,0,0) cm, (b) Reconstructed image using a single step, and (c) Reconstructed image after 5 nonlinear iterations.

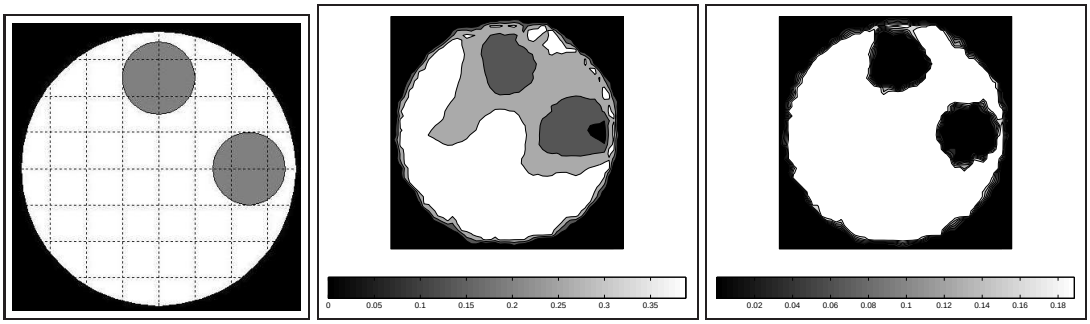

(a) (b) (c)

Figure 6: (a): Two inclusions with diameter of 4 cm centered at (0,5,0) cm and (5,0,0) cm with conductivity of 0.01 S/m, (b) Reconstructed image using a single step, and (c) Reconstructed image after 9 nonlinear iterations.

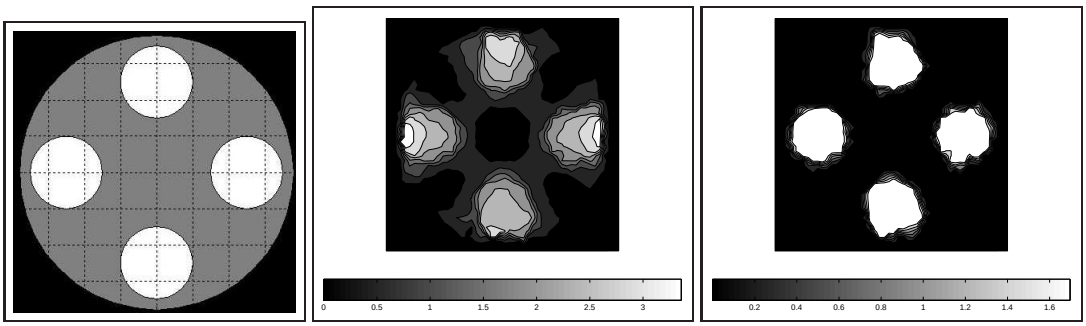

(a) (b) (c)

Figure 7: (a): Four inclusions each 4 cm in diameter with conductivity of 1.8 S/m centered at (-5,0,0) cm and (5,0,0) cm, (0,5,0) cm and (0,-5,0) cm, (b) Reconstructed image using a single step, and (c) Reconstructed image after 5 nonlinear iterations.

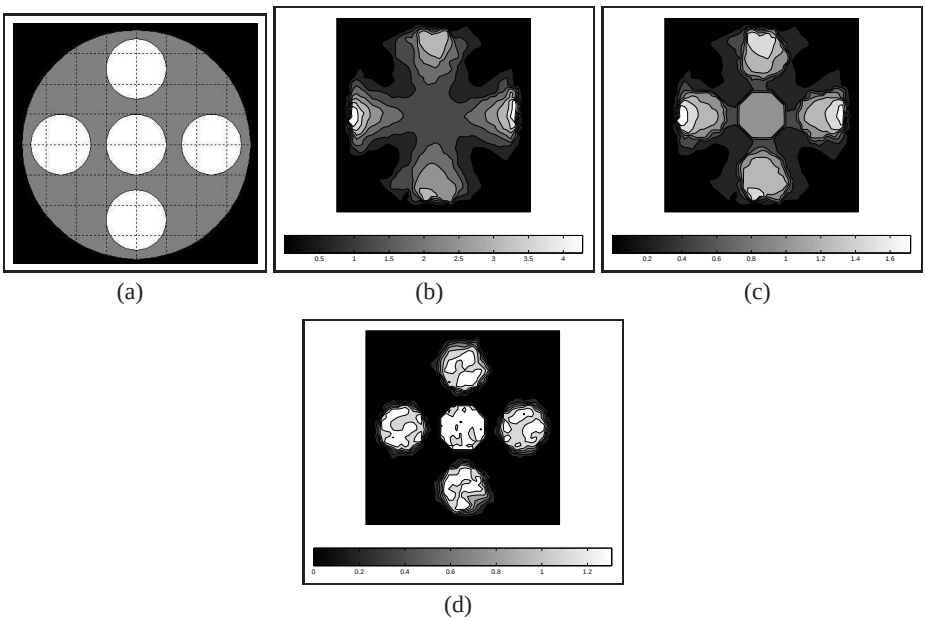

Figure 8: (a): Four inclusions with each 4 cm in diameter with conductivity of 1.3 S/m centered at (-5,0,0) cm and (5,0,0) cm, (0,5,0) cm, (0,-5,0) cm, and one at the center also with conductivity of 1.3 S/m (b) Reconstructed image using a single step, (c): Reconstruction after 2 iterations, and (c) Reconstructed image after 5 nonlinear iterations.

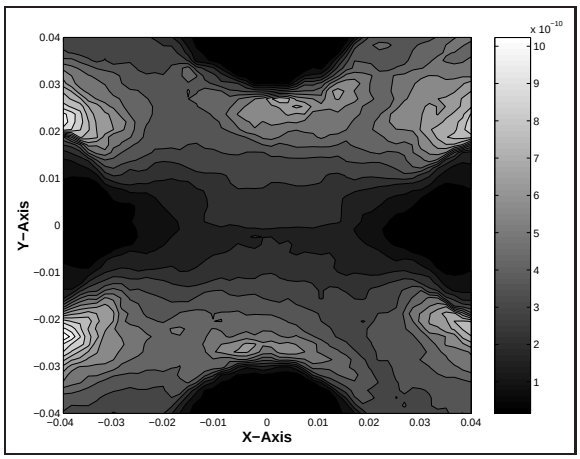

Figure 9: The sensitivity map for two opposite coils from the background conductivity distribution of Fig. 8.b, the values are in $V\Omega m$ for the electric current of $1\mathrm{Am}^{-2}$ in coils.

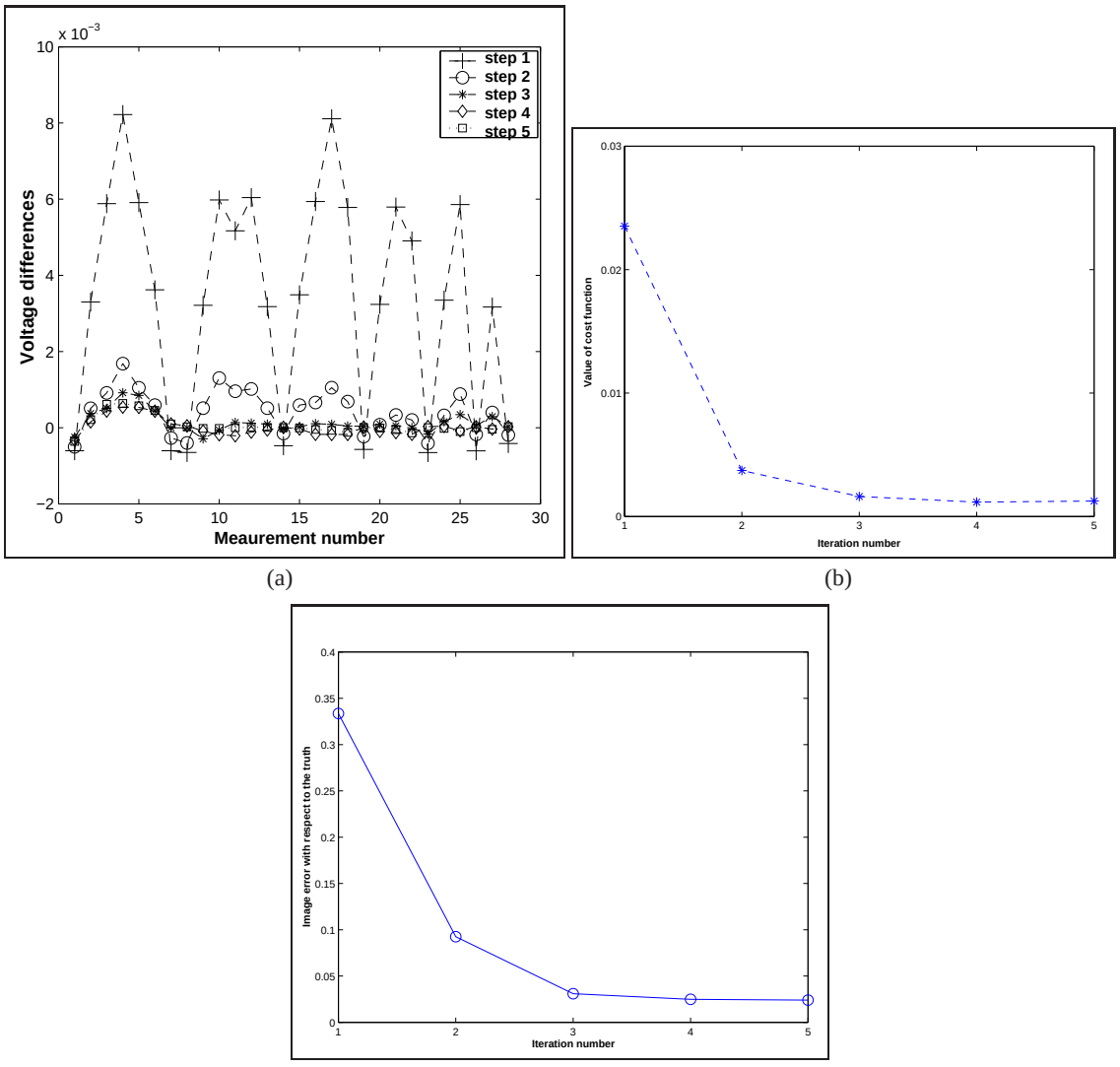

(a) (b)

(c)

Figure 10: (a) The differences between simulated and measured voltages over iteration steps, (b) The reduction of the cost function over the iteration steps, and (c) The improvement of the image quality during the iteration steps.